

Seasonal and spatial evolution of albedo in a snow-ice-land-ocean environment

Thomas C. Grenfell

Department of Atmospheric Sciences, University of Washington, Seattle, Washington, USA

Donald K. Perovich

Engineer Research and Development Center—Cold Regions Research and Engineering Laboratory, Hanover, New Hampshire, USA

Received 21 March 2003; revised 7 July 2003; accepted 30 September 2003; published 2 January 2004.

[1] In the course of a program studying Arctic coastal processes we have investigated the albedos for the range of surfaces in the region and their response to seasonal changes in a land-ice-ocean regime near Barrow, Alaska. From April through June in the years 2000, 2001, and 2002, spectral and wavelength-integrated albedos were measured along 200-m survey lines. These lines were installed at four sites and included sea ice, lagoon ice, fresh ice, and tundra. Initially, all sites were completely snow-covered, and the albedo was high (0.8–0.85) and spatially uniform. The concentration of absorptive contaminants in the snow was enough to produce a slight reduction below the pure snow values. As the melt season progressed, albedos decreased at all sites. The decrease was greatest and most rapid at the tundra site, where the albedo dropped from 0.8 to 0.15 in only 2 weeks. The spectral signature also changed as the wavelength of maximum albedo at the tundra site shifted from 500 nm for snow to 1100 nm for vegetation. As the snow cover melted, there was rapid and extensive ponding, resulting in a decrease of the spatially averaged, wavelength-integrated albedo from 0.6 to 0.2 in only 5 days. Extensive pond drainage and below-freezing temperatures caused the albedo to rebound briefly to 0.55 before resuming a steady decrease. Comparison of these results with data collected in the central Arctic show that albedos of fast ice in the coastal regime evolve significantly faster than pack ice albedos. Interannual seasonal variations showed additional melting phases that might be expected during protracted warming. The albedo evolution in the coastal lagoon was different each of the 3 years because of variations in sediment loading of the ice during freeze-up and in the melt/freeze pattern the following spring. The record early melt in May 2002 followed by a pronounced freezing event 2 weeks later produced a distinct melt regime that gave rise to reduced melt pond coverage and higher albedo. Such events provide insight into processes associated with the melt ponds that will be important for modeling sea ice in a warming climate. *INDEX TERMS:* 1863 Hydrology: Snow and ice (1827); 4850 Oceanography: Biological and Chemical: Organic marine chemistry; 1890 Hydrology: Wetlands; 3359 Meteorology and Atmospheric Dynamics: Radiative processes; 3360 Meteorology and Atmospheric Dynamics: Remote sensing; *KEYWORDS:* sea ice, lake ice, tundra, albedo evolution, spectral albedo, solar energy input

Citation: Grenfell, T. C., and D. K. Perovich (2004), Seasonal and spatial evolution of albedo in a snow-ice-land-ocean environment, *J. Geophys. Res.*, 109, C01001, doi:10.1029/2003JC001866.

1. Introduction

[2] There is substantial evidence that the Arctic climate is warming [Morison *et al.*, 2001]. The sea ice cover also shows signs of diminished thickness, extent, and seasonal duration over the last two decades [Rothrock *et al.*, 1999; Parkinson *et al.*, 1999]. Seasonal changes and short-term variability in the state of the ice cover and their effect on the interaction of solar radiation with the ice cover and underlying ocean are of particular importance in this context.

[3] Spring warming and summer melt rates as well as the length of the melt season are strongly influenced by the albedo, which decreases as the melt season progresses. Indeed, the ice-albedo feedback mechanism plays a key role in the heat and mass balance of the Arctic sea ice cover [Maykut and Untersteiner, 1971; Curry *et al.*, 1995]. To understand and model these processes, it is necessary to determine how shortwave radiation is distributed within the ice-ocean system and how this distribution affects heat and mass exchange within the system. Analysis of this system is complicated by spatial and temporal inhomogeneity of the summer ice cover, with surface conditions varying from

deep snow to bare ice to melt ponds to open leads, and with ice thickness ranging from zero (open water) to ridges tens of meters thick, all within an area that is often less than one square km. Each of these categories has a different set of physical and optical properties. To determine how average albedo changes over an extended area, we must examine both the temporal and spatial variability of albedo for each of the individual ice categories and monitor seasonal changes in the fractional area occupied by these categories.

[4] Because of the importance of albedo to the surface heat budget of sea ice, there have been a considerable number of studies defining wavelength-integrated and spectral albedos for a wide range of ice types and conditions [Langleben, 1969, 1971; Grenfell and Maykut, 1977; Grenfell and Perovich, 1984; Buckley and Trodahl, 1987; Perovich, 1991, 1994; Allison et al., 1993; Radionov et al., 1997; Hanesiak et al., 2001]. These studies have demonstrated that the variability of the albedo is linked to a strong dependence on surface conditions and the structure of the upper 30–50 cm of the ice. They have established a qualitative understanding of how changes in the physical properties of the ice and snow cause changes in the optical properties and the albedo. Most of these studies, however, do not provide systematic time series relating the seasonal evolution of albedo to changes in the surface conditions and physical properties of the ice. Because the optical properties of ice and snow as well as the incident solar irradiance are strong functions of wavelength, detailed wavelength-dependent observations are needed to determine the energy deposition. A detailed study of albedo versus ice type in shorefast first-year ice [Grenfell and Perovich, 1984] presented results for a wide range of sites and surface types, but the observations were limited by instrumental constraints to a few sites per day.

[5] In a recent paper [Perovich et al., 2002], a detailed time series was presented that demonstrates how the seasonal evolution of albedo in the central part of the Arctic Basin is linked to physical changes in the ice cover during melt and freeze-up. It is clear, however, from the general evolution of the ice in the coastal region that the presence of land modifies the temporal and spatial patterns of behavior. Complete meltout of the nearshore ice occurs followed by rapid retreat of the ice cover to distances of as much as hundreds of kilometers from the coast. This process has been accentuated in recent years and is believed to be driven in large measure by strong ice-albedo feedback.

[6] There has also been a considerable amount of theoretical modeling devoted to radiative transfer in snow and sea ice [Warren and Wiscombe, 1980; Grenfell, 1983, 1991; Perovich and Grenfell, 1981; Perovich, 1996; Light et al., 1998, 2003 manuscript in preparation, 2003]. These studies include detailed formulations suitable for the examination of the total and spectral albedos.

[7] In the coastal regime, the feedback processes are even more complex. Studies of ice anomalies and variability in the onset of ice melt in the coastal zone show that the individual components of the system may interact strongly with one another due to the differences in surface albedo between the prevailing surfaces (sea ice, tundra, lake ice) and the resulting contrasts in the input of solar energy. For example, the persistence of a thicker, high-albedo ice cover can suppress the amount of summer warming over the

tundra, while a thinner tundra snow cover may trigger negative ice anomalies through early onset of melt. The coevolution and interaction of the mass and energy balance of these different coastal surface types is largely unexplored. To understand and describe these processes quantitatively, we must determine how shortwave radiation is distributed within the ice-ocean system and how this distribution affects heat and mass exchange within the system. Such information is critical to understanding the role of the ice cover in the climate system and its importance as indicator and modulator of climate variability and change.

[8] In this paper we present results from studies done at Barrow, Alaska, in 2000, 2001, and 2002 investigating the albedos of the land, sea ice, lake ice, and ocean environments. These investigations include detailed time series at a variety of sites from winter conditions through the final stages of decay of the ice and snow. The time of primary interest was the spring melt season when temporal changes are large, conditions are highly nonuniform, and interactions between the ice, ocean, and atmosphere are greatly accelerated.

2. Instruments and Methods

[9] Spectral and wavelength-integrated albedos were measured from November 1999 through June 2002 at four sites including tundra (Tundra), a freshwater lake (Imikpuk Lake), a seawater lagoon (Elson Lagoon), and shorefast sea ice (Chukchi Sea). These sites were selected to encompass the wide range of surface conditions found in the Barrow area. The locations of the sites are indicated on the map in Figure 1.

[10] Spectral and wavelength-integrated albedos were measured along selected survey lines 200 m in length. These “albedo lines” allowed us to investigate the small-scale spatial variability of albedo and to determine a spatially averaged albedo for the four different sites. Spectral and wavelength-integrated albedos were measured along the lines at a spacing of 5 and 2.5 m, respectively. Initial observations were made under winter conditions in early April and then every 2–4 days from late May through June, covering the bulk of the melt season. The spectral albedo at a particular wavelength (λ) is

$$\alpha(\lambda) = \frac{F_{\uparrow}(\lambda)}{F_{\downarrow}(\lambda)}, \quad (1)$$

where $F_{\downarrow}(\lambda)$ is the incident spectral irradiance, including direct solar and diffuse contributions, and $F_{\uparrow}(\lambda)$ is the upwelling spectral irradiance scattered by the surface upward into the atmosphere. Spectral albedos from 350 to 2500 nm were measured using an Analytical Spectral Devices FieldSpec Pro spectroradiometer. The instrument had a response time of less than a second, allowing a pair of incident and reflected scans to be recorded in less than 10 s, minimizing drift due to changes in the incident irradiance. As a result of the strong atmospheric water vapor absorption from 1800 to 1950 nm and beyond 2200 nm, the incident radiation is reduced to very low levels in these wavelength bands. This resulted in gaps in the spectral albedos, particularly on cloudy days when the incident radiation was lower and the atmospheric water content was higher.

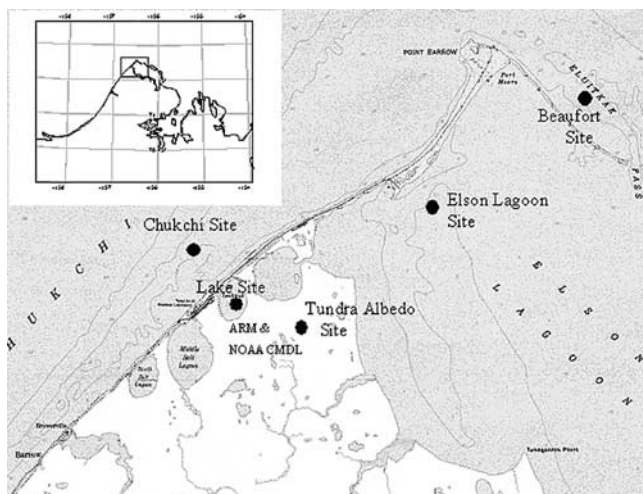


Figure 1. Experimental area and the location of the albedo sites.

[11] The wavelength-integrated, or total, albedo (α_t) is the ratio of the reflected solar irradiance (F_r) to the incident solar irradiance (F_i), which is given in terms of the spectral albedos by

$$\alpha_t = \frac{\int_{300}^{3000} \alpha(\lambda) F_i(\lambda) d\lambda}{\int_{300}^{3000} F_i(\lambda) d\lambda}, \quad (2)$$

where the limits of integration span the incident solar spectrum. Albedos integrated from 300 to 3000 nm were measured using a Kipp and Zonen albedometer, which has a time constant of approximately 10 s. Both instruments were mounted on a 1.5-m-long horizontal arm and deployed about 1 m above the surface to minimize the effects of shadowing. With this configuration, the shadowing was estimated to be less than 0.5%.

[12] In addition to the albedo measurements, selected physical properties of surfaces at the sites were also monitored in detail. These include snow coverage and depth, the melt pond fraction and depth, the evolution of the ice surface scattering layer, and the fraction of exposed vegetation. Photographs were taken with each set of albedo measurements to document changes in surface conditions. Because the surface layers of snow, ice, and tundra are either highly scattering or strongly absorptive, the surface conditions have the greatest influence on albedo [Grenfell and Maykut, 1977; Perovich, 1996; Allison *et al.*, 1993].

[13] Contamination of the snow by soot and dust was investigated at each site using the method employed by Grenfell *et al.* [2002]. Bulk snow samples of 1 to 3 liters were melted and filtered through 0.4- μm nuclepore filters. The filters were analyzed using a four-channel integrating plate photometer, described by Bond *et al.* [1999], to determine the reduction in transmissivity relative to clean filters produced by the deposited contaminants. The impurity concentration results are expressed in specific mass of

filtrate per unit mass of snow. These values depend on the assumed absorption efficiency of the particles in question. We used a value of $6 \text{ m}^2/\text{gm}$, but the precise value is not critical in the present context because the filter transmissivities provide a measure of the effective optical properties of the material that can be used directly in radiative transfer modeling of the snow. We have expressed the results in terms of equivalent soot concentration (ng C/g) at 525 nm using the same absorption efficiency so that the present values can be compared directly with the SHEBA results of Grenfell *et al.* [2002]. A value of 15 ng C/g is considered to be the threshold level at which the contaminants will produce a measurable effect on albedo at 525 nm.

3. Results

3.1. Measurement Sites

[14] Photographs taken before and after the start of melt at each of the four observation areas are presented in Figure 2. For much of the year, these disparate sites are covered by an optically thick layer of snow, and the albedo is quite similar and spatially very uniform. During the melt season, however, there is considerable spatial variation at each site as the snowmelts, exposing the underlying material, and differences between the sites become quite pronounced. The timing and duration of the melt period is of critical importance in the local and regional energy balance because the surface conditions then become highly nonuniform and the resulting horizontal gradients accelerate the interactions between the land, ice, ocean, and atmosphere.

3.2. Physical Properties

3.2.1. Snow

[15] Extensive snow depth measurements were made at each of the four sites. Late winter readings were obtained near the time of maximum accumulation in April 2000, 2001, and 2002. They are presented in Table 1 along with the date when the snow cover had melted at the Chukchi site. In all 3 years the snow was deepest at the Tundra site, resulting from the topographic relief of the underlying surface, which was the largest of all the sites selected. The snow depth showed the least amount of interannual variation on Imikpuk Lake because of the uniformly smooth topography from year to year. For 2 of the 3 years, the snow was shallowest at the Chukchi site.

[16] The contaminant loading of the snow in April is shown in Figure 3a. It was generally highest at the Chukchi site and tended to decrease at the sites that were further north or upwind of the roads which were plowed free of snow in the winter. For the 2002 season, the Chukchi site was located further offshore in a cleaner area, resulting in a corresponding decrease in the contaminant level. The spectral transmissivities of the filters (Figure 3b) were greatest at 435 nm with a marked decrease as the wavelength increased to 800 nm, characteristic of a brown or reddish brown material as compared with soot, whose spectrum is relatively flat over this wavelength range. The contaminant loading of the snow thus appears to have included a substantial fraction of windborne dust from the nearby road, while the soot loading was comparatively low. More detailed analysis of the filters would be needed to determine the relative concentrations of dust and soot.

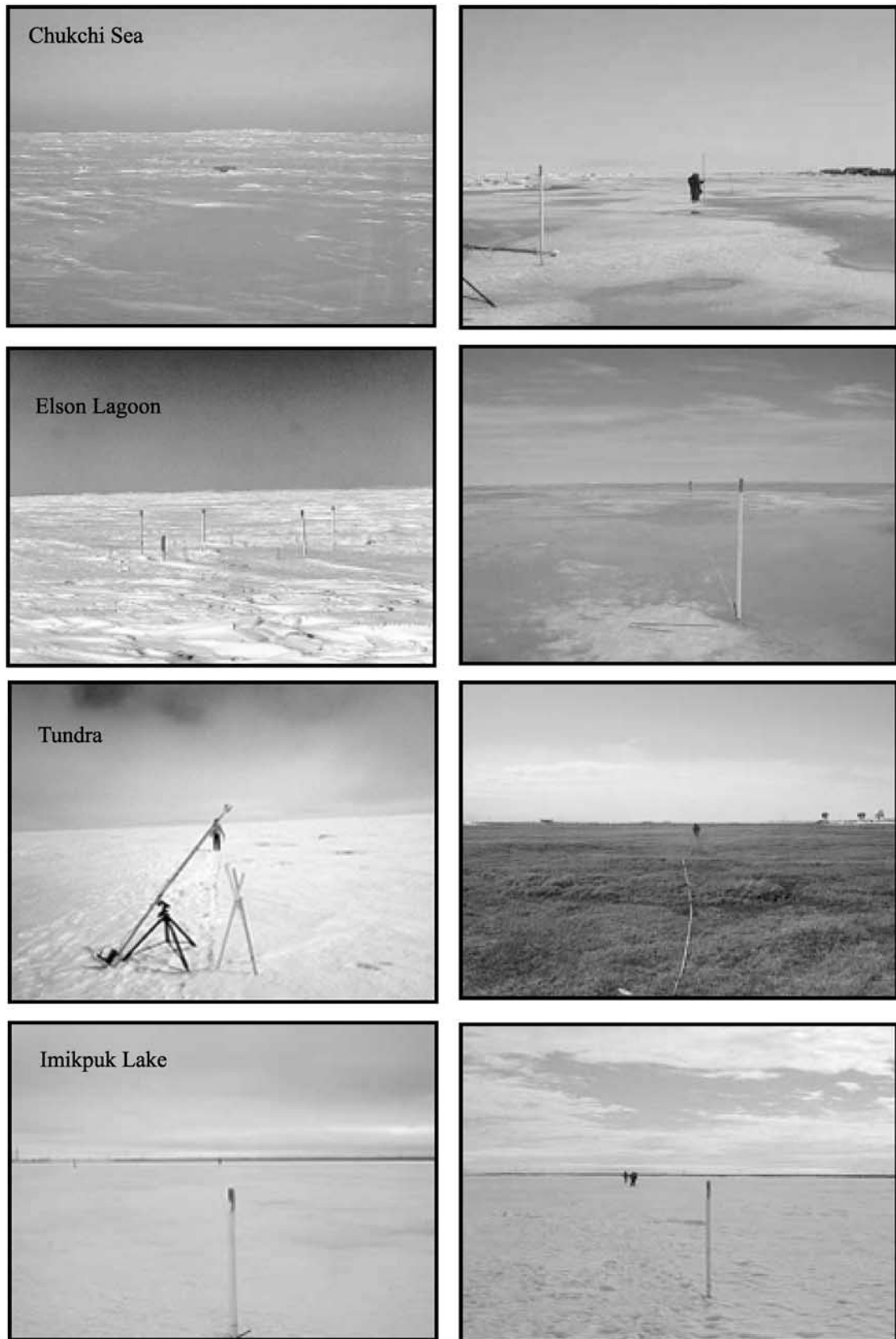


Figure 2. Photographs of the four albedo sites illustrating conditions during the growth and melt seasons. See color version of this figure at back of this issue.

Table 1. Average Snow Depth (From 600 Observations) in April at Each Observation Site and the Date When the Snow Melted Away at the Chukchi Sea Site^a

Year	Tundra	Elson Lagoon	Chukchi Sea	Imikpuk Lake	Date of Disappearance of Snow From Chukchi Site
2000	0.28	0.27	0.23	0.19	12 June
2001	0.29	0.20	0.12	0.20	13 June
2002	0.26	0.23	0.12	0.19	24 May

^aDepths are in meters.

[17] The contamination levels are such that the effect on the visible albedos was less than about 4%, with the greatest influence at the Chukchi site in 2000 and 2001. These values are only slightly larger than those reported by Grenfell *et al.* [2002] for the central Beaufort Sea during the SHEBA experiment and significantly lower than values obtained in the 1980s [Clarke and Noone, 1985], indicating that the temporal decrease in soot contamination since that time has occurred in the vicinity of Barrow as well as in the central Arctic.

3.2.2. Sea Ice

[18] For the purpose of understanding the albedo of first-year ice, the structure of the sea ice can be broadly characterized by up to three distinct layers depending on season. There will be some variability of the inherent optical properties of each layer. This will be addressed in more detail below.

[19] In winter, there was a snow layer over fairly homogeneous ice. Laboratory studies with ice cores have shown that vertical variations in salinity and temperature do not appear to produce a strong influence on the optical properties of sea ice above the eutectic temperature (-22.4°C) as long as the brine does not drain from the ice (B. Light *et al.*, manuscript in preparation, 2003).

[20] When the melt season began, most of the brine drained out of the upper layers of the ice, producing a "surface scattering layer" that persisted throughout the melt season and tended to maintain the albedo of unponded ice at

a fixed level. The thickness of this layer is determined by a balance in the rates of surface ablation due to the surface heat fluxes and the rate of internal melting and brine drainage due to the absorption of shortwave radiation. The same effect has been reported for the central Arctic by Perovich *et al.* [2002]. This surface scattering layer was sometimes covered with snow to produce a three-layer system, but during most of the melt the snow was absent.

[21] The structure of a representative core is shown in Figure 4. The drained surface layer, which was about 10 cm thick, is apparent in the photograph. The uppermost 3 cm, the surface scattering layer, was a decomposing granular layer for which the granules ranged in diameter from about 1 mm to 5 mm, increasing with depth below the surface. The contrast with the lower part of the core is probably somewhat accentuated because of excess brine drainage that occurred when the core was extracted. Additional drainage features quickly developed where the core broke, but within the ice sheet the optical properties of these areas were essentially the same as the rest of the interior ice.

[22] In areas where the ice was depressed, meltwater tended to collect, producing melt ponds. Initially, the meltwater spread out over most of the surface, producing a fractional cover of melt ponds in excess of 50%. As melting developed, a series of channels developed on the surface, allowing the pond water to drain through cracks and porous areas of the ice. The pond fraction was greater at Elson Lagoon than at the Chukchi site: the ice topography at

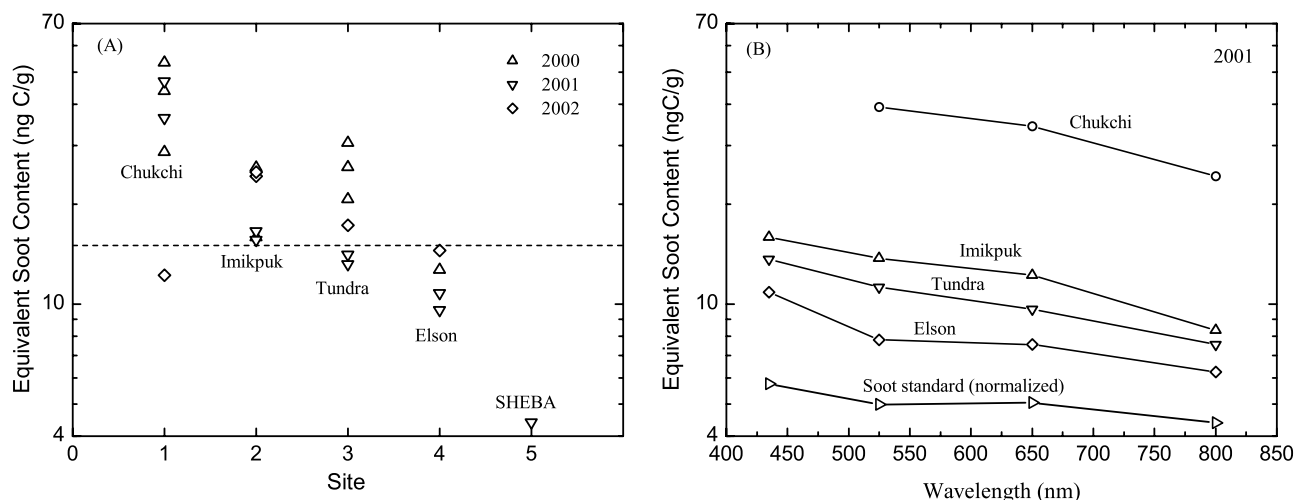


Figure 3. Contaminant loading of snow: (a) the equivalent soot content (ng C/g) at 525 nm for the various sites during the 3 years of the experiment and the average value from the SHEBA observations and (b) spectral absorption signatures of the contaminant on the filters for 2001. The curve for the soot standard was arbitrarily normalized to fit on the graph. The threshold of detection for albedo at 500 nm is approximately 15 ngC/g equivalent (dashed line in Figure 3a).

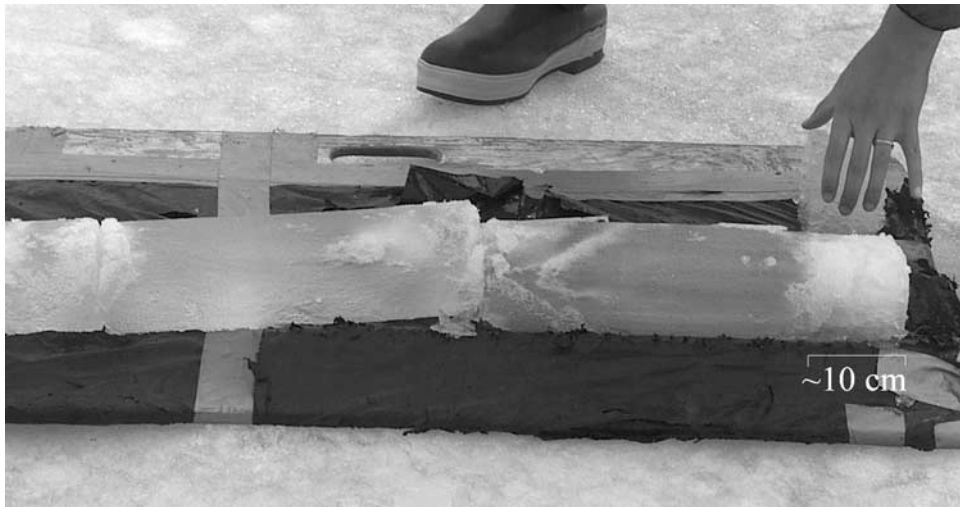


Figure 4. Sea ice core from drained bare ice in Elson Lagoon, June 2002. The top of the core is to the right. The surface scattering layer is about 10 cm thick.

the lagoon was level because of the absence of pressure ridging and buckling. The ice in the ponds was quite porous at the base of the meltwater layer, but the pore spaces were filled with water and there was no visible optical layering.

3.2.3. Lake Ice

[23] The structure of the lake ice was significantly different from that of sea ice because of the lack of submillimeter inhomogeneities due to brine inclusions. As a result, volume scattering in the fresh ice was significantly smaller, producing lower albedos over areas where the snow cover was thin or absent.

[24] With the onset of melting, the lake ice decayed by melting at crystal boundaries, and the horizontal size of individual crystals was on the order of centimeters. These crystals were much more elongated in vertical extent, approaching 10–20 cm in some cases, producing a candling pattern that was spatially uniform across the entire surface of the lake. This resulted in a complex network of subsurface channels that allowed meltwater to percolate horizontally. As a result, the melt ponds on the lake were initially quite shallow because the surface was flat and intact; however, as the candled structure developed, the meltwater quickly sank below the surface and percolated into cracks or off the edge of the ice. At this point, the melt pond coverage dropped to almost zero and remained that way throughout the course of our experiments.

[25] The same process occurred in the refrozen melt ponds at the sea ice sites in 2002. Because the melt pond water was fresh when it froze, the ice developed the same candled structure as the lake ice when the melting resumed. In addition, even though the surface refroze, the interior ice continued to absorb solar radiation and increase in porosity. As a result, both the lateral and vertical transport of water were enhanced, so that when melting restarted, the area covered by ponds was less than before and the second generation melt ponds often formed in new locations.

3.3. Spatial Variability

[26] Figure 5 shows wavelength-integrated albedos, α , measured along the albedo lines at the four sites from late winter and as the melt progressed during 2001. Because the

surfaces were covered by an optically thick layer of snow, there was little spatial variability in albedo before melt began and little variation from site to site in general. Each of the Elson Lagoon, Tundra, and Chukchi Sea albedo lines had an albedo of about 0.8. Portions of the Imikpuk Lake albedo line were snow-free because of wind scouring of the smooth ice surface. The albedo of the bare ice segments was about 0.3. The albedo of the lake in general was slightly less than the other sites because of the thin snow cover.

[27] As the snow cover began to melt, there was a general increase in the spatial variability of the albedo at all sites. During the transition to complete snowmelt, the variability in albedo was greatest at the tundra site because the contrast in albedo between melting snow and tundra was larger than between snow and melting sea and lake ice.

[28] When snowmelt was complete, the Elson and Chukchi sites were a mix of bare ($\alpha = 0.6$) and ponded ($\alpha = 0.2$) ice, whose spatial variability was large. Before the ice surface began to melt, the fresh ice at Imikpuk Lake did not have a surface scattering layer. As a result, bare surface albedos were for the most part between 0.3 and 0.4. As the surface scattering layer developed, the albedo increased to about 0.7 and was again rather uniform. As the ice thinned, the albedo decreased but remained spatially uniform because of the lack of melt ponds. Tundra albedos were spatially uniform over the exposed soil (0.15 to 0.2), but wet areas and ponds had lower albedos.

3.4. Seasonal Evolution

[29] The temporal evolution of areally averaged albedo during the 2001 season is shown in Figure 6. Prior to the onset of the melt season, albedos at all four sites were similar because of the snow cover. Area-averaged albedos for Imikpuk Lake and the tundra were slightly lower because of thin spots in the snow cover. As melt progressed, albedos decreased at all sites. There was a rapid decrease at the tundra site from 0.8 to 0.15 in less than 2 weeks. Melt pond formation reduced albedos at the Chukchi and Elson sites, and once the snow cover was gone, shallow melt ponds formed over a wide area, causing the albedos at the sea ice sites to decrease further. As soon as drainage through

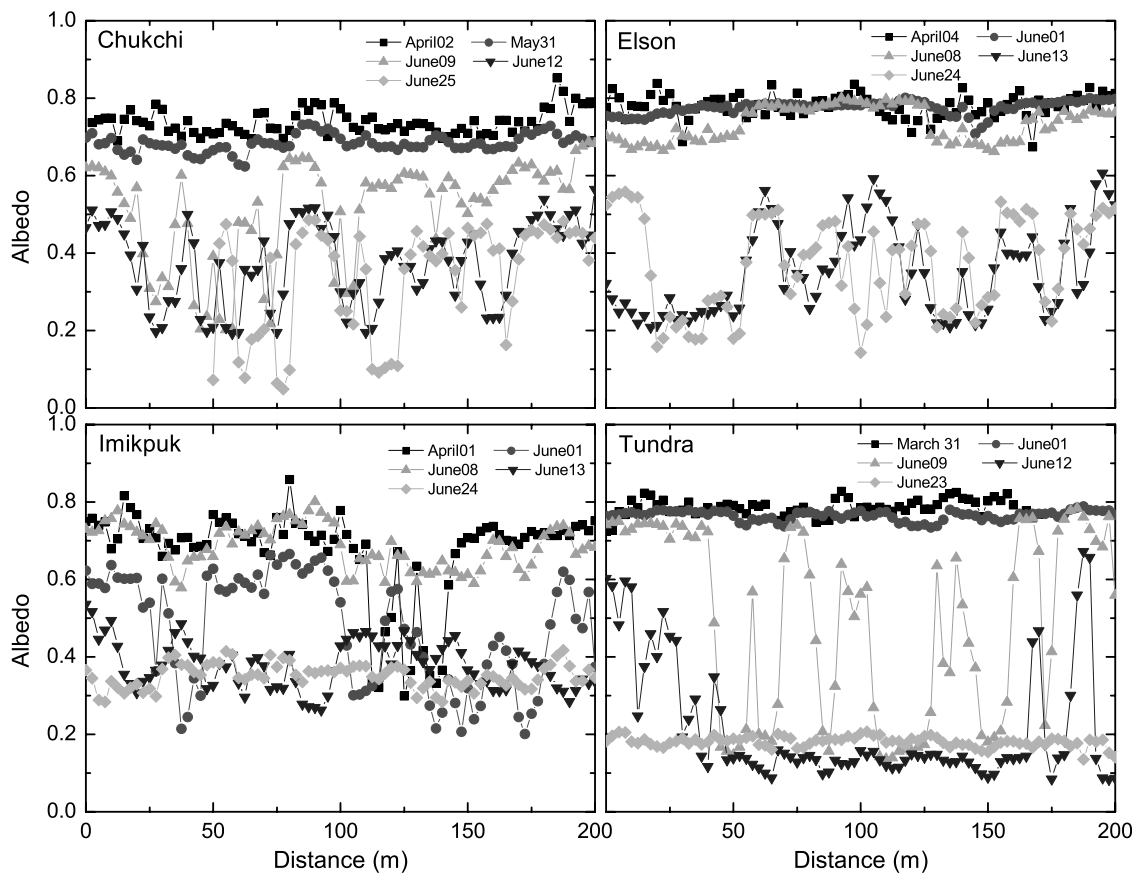


Figure 5. Spatial variability of albedo observed at the four sites during the spring-summer 2001. Imikpuk Lake has the lowest April albedo since it has the thinnest snow cover. See color version of this figure at back of this issue.

the ice was established, the melt pond area decreased rapidly with a corresponding rise in albedo, for example, on 8 June 2001 (see Figure 6). The sea ice albedos were influenced by subsequent variations in melt pond development. The albedos decreased with broadening and deepening of the ponds as melting progressed and increased briefly with the formation of an ice skim on the surface with some snow deposition. The average snow-free albedos were largest for the lake site because of the formation of a thick drained surface layer, while tundra albedos were smallest because of the low albedo of the vegetation. There was a cold spell from 15 to 22 June when albedos at the ice sites increased as the upper 1–3 cm of the ponds froze and were coated with a light dusting of snow. After this the melting resumed, with an accompanying decrease in the albedos.

[30] The albedo decrease on shorefast, first-year sea ice occurred much faster than that observed on multiyear pack ice at SHEBA. It was accelerated by melting due to thermal interaction/lateral heat advection from the nearby land. A significant amount of heat was also deposited in the water in the nearshore lead, a portion of which was transported to and under the shorefast ice, contributing to lateral melting and to the oceanic heat flux. While the thinning of the ice did not produce a significant reduction in the albedo directly, it did contribute to the more rapid decay and disappearance of the ice cover.

[31] There is a degree of temporal complexity in the general reduction of sea ice albedo that was particularly

evident at the Elson Lagoon site in 2001. Figure 7a shows the transition from a patchy snow cover on 11 June to almost 100% shallow melt pond cover on 15 June, followed by a mosaic of drained areas and deeper melt ponds on 18 June. Figure 7b shows the albedo versus fractional pond coverage in the field of view of the instrument. The pond coverage was estimated on site by eye for each observation along the lines to provide a way to estimate the albedos of the pure surface types, particularly because ponded and drained ice areas often did not fill the field of view of the instruments. For the three different cases, whose spatially averaged albedos were quite different, the pure bare ice and melt pond albedo values were approximately 0.6 and 0.2, respectively. As we found for multiyear ice during SHEBA [Perovich *et al.*, 2002], the drained ice albedo remained nearly constant during the melt season although the value for multiyear ice were slightly higher. This supports the model that the regional albedo of melting sea ice is controlled primarily by the melt pond development and fractional coverage.

[32] The seasonal evolution of spectral albedo in 2001 is presented in Figure 8 as spectra averaged over the 200 m lines at each site. As the snow melted, spectral albedos exhibited a general decrease for all wavelengths and, except for the tundra site, this continued as the melt season progressed. For bare and ponded ice, the maximum albedo was between 450 and 550 nm and the general spectral shape was similar to previously reported observations [Grenfell *et*

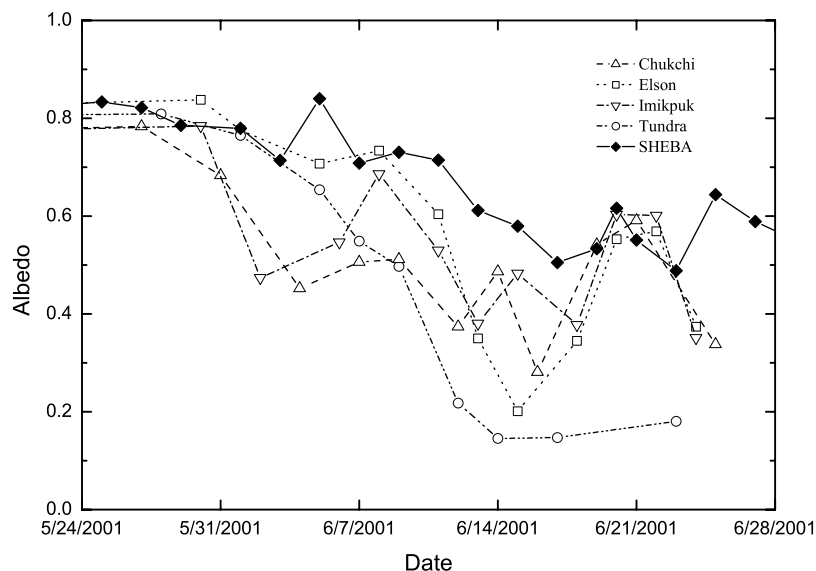


Figure 6. Evolution of wavelength-integrated albedo. Values averaged over a 200-m-long albedo at each of the four sites are presented. Results from Arctic pack ice (SHEBA) are also presented [Perovich *et al.*, 2002].

al., 1994; Perovich *et al.*, 2002]. The spectral albedo for bare tundra was quite distinct from that of ice and snow, with maxima at about 1100 and 1300 nm. Thus, as the snow melted at this site exposing the tundra, the visible albedos decreased sharply while near-infrared values between 1300 and 1700 nm increased. As the season progressed and the vegetation began to grow, the visible albedos remained approximately constant and the infrared albedos continued to increase.

3.5. Interannual Variability

[33] Figure 9 shows a comparison of the evolution of total albedo during the melt for the three study years. In 2000 and 2001, the onset of melt on the ice occurred within a day of one another, on 31 May and 30 May, respectively. In 2002, however, the melt onset occurred in mid-May, about 2 weeks earlier. The general trend in all years was a decrease in albedo as the melt season progressed, modulated by freezing events.

[34] The first evolutionary stage was associated with coarsening of the snow grains and melting of the snowpack. At the tundra site this was the dominant process, and it took about 2 weeks to complete in all 3 years. Since the snow thickness was greatest at this site, snow-covered areas lasted longer there. At the Chukchi site, the snowpack melted in about 7–8 days in both 2000 and 2001, and in 2002 it had disappeared before 24 May, 10 days after melt onset.

[35] In 2000, except for a few brief periods of cooling, the melt was steady, and in general the albedos decreased until just before breakup of the ice. At Elson Lagoon, sediment had been mixed by a storm throughout the water column during freeze-up and was included in the upper 10–20 cm of the ice. The resulting bare ice albedo was low and accelerated the melting, decreasing the albedo further to a level comparable with that of the tundra.

[36] In 2001, the albedo decrease during the melt was interrupted by a freezing event with snowfall lasting about 3 days (~10 June) and a second event 10 days later. As in

the previous year, the new snow melted much more rapidly at the tundra site and its albedo was affected only slightly. The sea ice at Elson Lagoon was not sediment-laden in 2001 and the snowpack was thicker. Its albedo followed those of the other ice sites much more closely.

[37] The 2002 season was quite unusual. The onset of melt date was the earliest on record over the past 40 years. Melt ponds had formed by 24 May. By the end of May, the melt ponds reached maximum extent at the Chukchi site, and the melting of snow was essentially complete at all sites. The resulting runoff from the tundra snowpack produced flooding of the Elson Lagoon site. The water depth exceeded 40 cm at the maximum but subsided to about 20 cm by 27 May. At that point a strong freeze event set in, accompanied by 3 cm of snowfall on 1 June, and the temperatures remained below freezing until 4 June. At the tundra site, the surface was snow-free beforehand and it had begun to warm, so the new snow melted rapidly and the increase in albedo was less than 0.05. At the lake ice site, melting ceased, the subsurface water drained away or refroze, enhancing the surface scattering layer, and there was some new snow. All of these combined to increase the mean albedo to 0.82. At the sea ice sites, the ponds and the flood water froze to the bottom and the snowfall raised their albedos to about 0.75.

[38] After 4 June, the melting resumed and continued uninterrupted until breakup on about 8 July. The melt ponds appeared again on the sea ice, but the decay of the fresh ice from the previous ponds was characterized by candling as for Imikpuk Lake, rather than the decay into smaller-scale (1–5 mm) granular structure more representative of sea ice. As a result, the size and distributions of the new melt ponds were quite different from the first, and the ponded area was significantly less. This gave rise to the general increase in the ice albedos from 11 to 20 June.

[39] The fast ice deteriorated by late June each year after about 4 weeks of melting. The actual retreat from the coast, however, depended on the occurrence of the appropriate

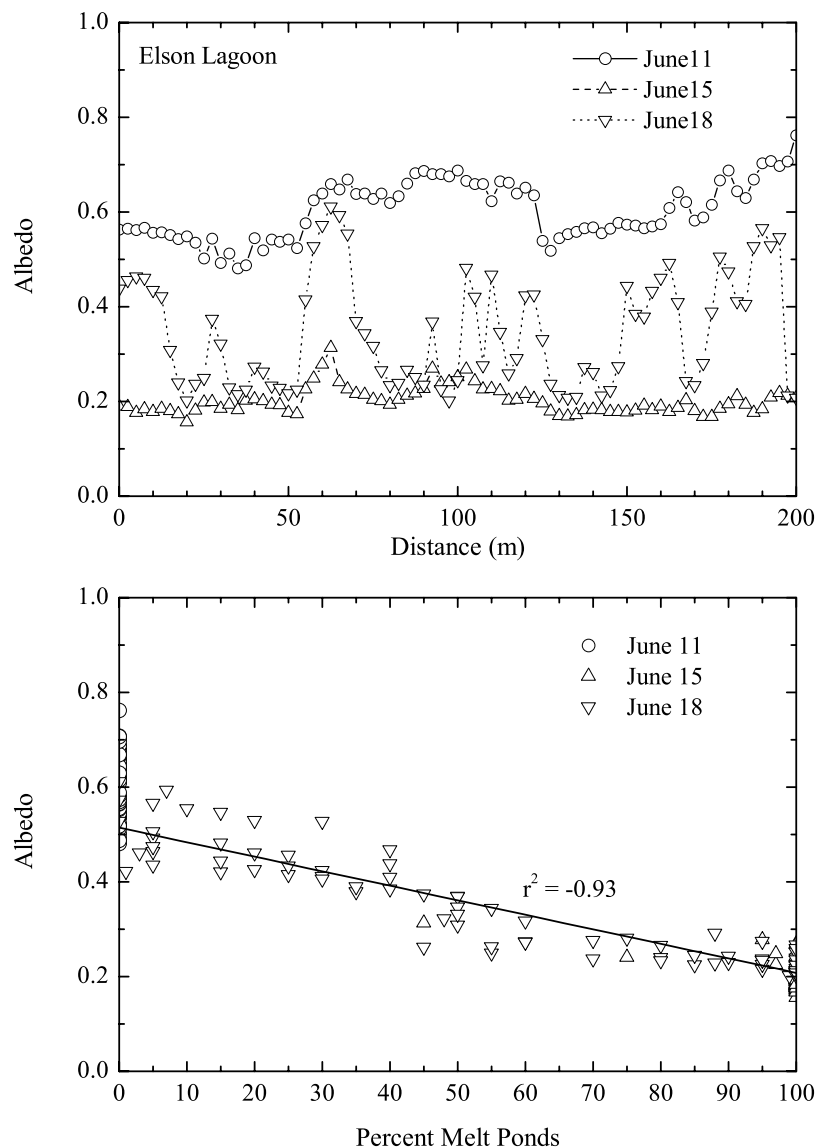


Figure 7. (a) Evolution of the horizontal transect profile for wavelength-integrated albedo measured at the Elson Lagoon site in 2001. (b) Albedo versus percentage of surface covered by melt ponds in the field of view of the instrument. The solid line is a linear regression to the data of 18 June, for which $r^2 = -0.93$.

offshore wind conditions. The dates of breakup are given in Table 2, at which point the albedo decreased to the value for open water of about 0.07 consistent with the results of *Pegau and Paulson* [2001].

3.6. Spectral Signatures

[40] The spectral signatures of the predominant surface types are shown in Figure 10. Although the spatiotemporal averaged albedos of bare melting sea ice were quite constant, there were significant spectral differences in albedo for various surface types arising from local differences in snow cover, contaminant loading, and strong melting events. Over the spectral region from 400 to 1400 nm, cold snow had the largest albedo. For snow and ice, the maximum albedo was in the 450- to 550-nm range. The peak was narrower for melt ponds because of the weaker back scattering near the surface and greater penetration, enhanc-

ing the influence of absorption on the upwelling radiation. The albedo for dirty ice had a broad maximum from 600 to 900 nm, but the specific shape of the spectrum for this type depends on the concentration of the dirt/sediment. These albedos are generally consistent with observations during previous experiments.

[41] For bare tundra, the spectral albedos were low at visible wavelengths, increasing steadily with increasing wavelength from 0.01 at 400 to a maximum value of 0.42 at approximately 1300 nm in the near infrared. Secondary maxima were recorded at 1100 and 1650 nm. Wet tundra had a lower albedo, in general, because of the reduction of scattering by water filling in interstitial spaces combined with the strong absorption in the infrared. Also the maximum at 1100 nm that was greater than the peak at 1300 nm because of the enhanced absorption at longer wavelength by the extra water. Further into the infrared, the tundra albedos

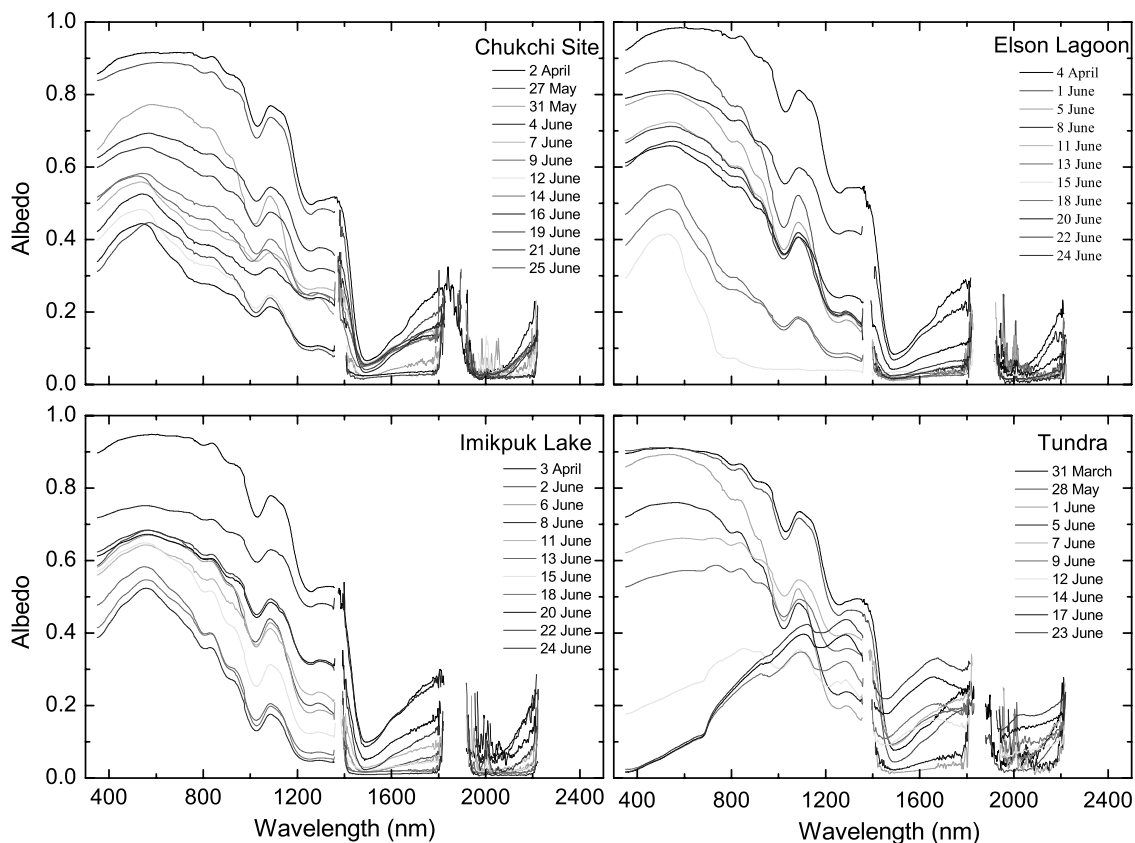


Figure 8. Evolution of mean spectral albedo at the four sites. Each curve represents the averaged value of albedo over a 200-m-long line. The decrease as the melt season develops is clearly apparent. See color version of this figure at back of this issue.

dropped sharply between 1350 and 1450 nm and again between 1800 and 1900 nm in response to the strong infrared H_2O absorption bands.

3.7. Incident Spectral Irradiance and Total Albedos

[42] Figure 11 presents incident solar irradiance spectra for representative clear and cloudy conditions at polar latitudes. Because calibration problems precluded the direct use of incident radiation observations, the spectra used here are averages from several cases of clear sky and uniform overcast under melt conditions taken from recent field experiments and currently used in our radiative transfer model [Grenfell, 1991]. The revised incident irradiance spectra are more accurate than those presented in the original paper and have not been previously published. Total albedos computed from the spectral albedos in Figure 10 are presented in Table 3.

[43] The difference in integrated albedo with illumination conditions is a significant perturbation. The incident spectral irradiance in equation (2) weights the visible wavelength region more strongly on cloudy days when the infrared component of $F_1(\lambda)$ decreases relative to the visible component (Figure 11), so the total albedo for snow and ice surfaces is larger on cloudy days. For the snow and ice surfaces considered here, the difference ranges from 0.077 for the cold snow to 0.012 for a mature melt pond. For open water, whose spectrum is essentially flat, $\Delta\alpha$ is negligible. Note that for the tundra sites $\Delta\alpha$ is negative. This effect has

been discussed in detail earlier [Grenfell and Maykut, 1977; Grenfell and Perovich, 1984], but the values reported were slightly larger than those presented above because of limitations in the knowledge of the incident spectral irradiance, particularly for cloudy conditions.

4. Discussion

[44] Because the physical and optical properties of the ice beneath the snow are essentially constant during the winter, we can examine observations up to the onset of melt to test the depth of the snow for which the albedo reaches an asymptotic value. By considering a case with an underlying surface whose albedo is small and comparing observed albedo with snow thickness, we can see how thin the snow layer must be for the albedo to decrease detectably. The Imikpuk Lake site was the best example because it offered the combination of a low spatially uniform snow-free albedo (0.35 for cold ice and 0.30 at the onset of melt) with the thinnest snow cover. Figures 12a and 12b show the results from 7 April 2000 and 30 May 2001 before the snowpack had begun to melt. The characteristic snow grain radius at this time was approximately 0.1 mm. The albedo of the snow cover was very close to 0.80 for snow depths greater than 10 cm, but for thinner snow the albedos began to decrease. The results for both cases have been fitted to the same empirical exponential curve and indicate that albedo saturation occurred at 6–7 cm snow thickness. We

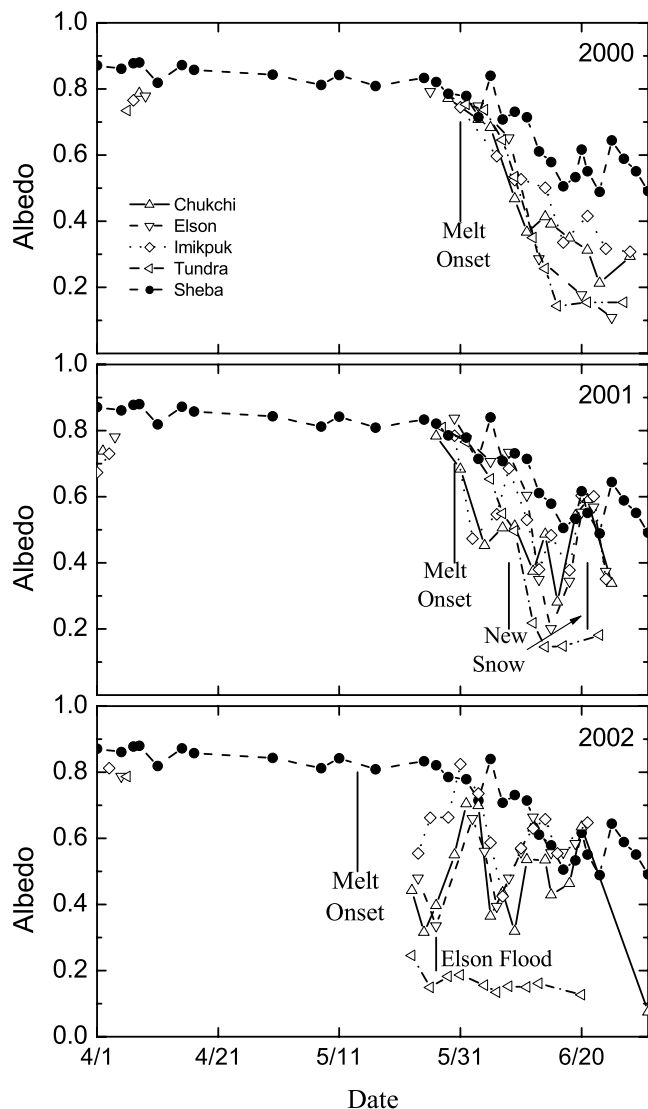


Figure 9. Seasonal evolution of wavelength-integrated albedo for 2000, 2001, and 2002. Values averaged over a 200-m-long albedo at each of the four sites are presented. Results from pack ice in the central Arctic [Perovich *et al.*, 2002] are also shown (black circles plus dashed line).

assume this corresponds to an extinction optical depth of about 4, which attenuates more than 98% of upwelling irradiance from the base of the snow layer. Since the optical depth equals ($K \cdot z_{\text{snow}}$), the effective irradiance attenuation coefficient, K , was approximately 0.6 cm^{-1} .

[45] Figure 12c shows the corresponding results from Imikpuk Lake on 2 June 2001 just after melting had begun. In this case, the snow grains had metamorphosed to nearly

Table 2. Dates of Ice Breakup

Year	Chukchi Coast First Ice Free ^a	Web Camera Data, All Ice Gone From Coast
2000	12 July	12 July
2001	2 July	20 July
2002	8 July	15 July

^aC. George (personal communication, 2002).

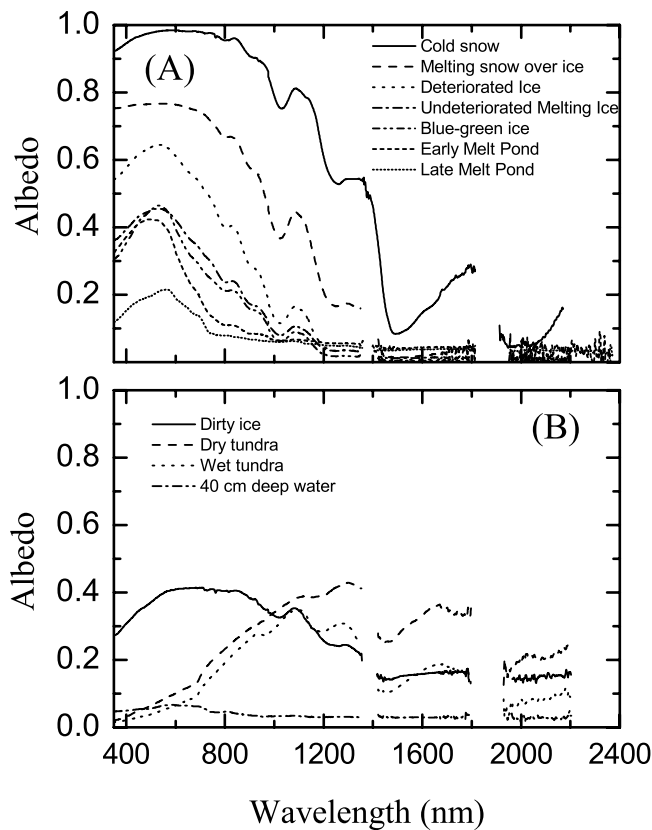


Figure 10. Spectral albedos of surface types representative of conditions in the snow-ice-land-water environment of Barrow, Alaska.

spherical shapes with grain radii of 0.5 to 1 mm, and some meltwater had reached the surface of the ice in some areas, decreasing the albedo to as low as 0.2. The asymptotic albedo for thick snow also decreased to about 0.65 and the saturation thickness doubled, to 10 to 12 cm, indicating that the transmissivity of the snow layer had increased and that $K \approx 0.3 \text{ cm}^{-1}$.

[46] Calculations by Wiscombe and Warren [1980] and Warren and Wiscombe [1985] indicate that the albedo of snow over a darker underlying layer should begin to decrease for liquid equivalent values of 2 and 10 g/cm^2 for snow grain radii of 0.1 and 1 mm, respectively. Assuming snow densities of 0.34 and 0.4 g/cm^3 , the values for the present case, the saturation snow depths would be about 6 and 25 cm for new and melting snow. The results of Wiscombe and Warren [1980] for new snow correspond quite well with the present observations in Figures 12a and 12b. Their values for melting snow, however, assume a grain size that is twice as large as the results in Figure 12c, and the saturation depth they predict for this case is correspondingly larger. Their results bracket the present cases and are consistent with our observations.

[47] The onset of melting at SHEBA (28 May) occurred at almost the same time as at Barrow in 2000 and 2001; however, as indicated by Figures 6 and 9, the albedo progression at SHEBA was slower and more uniform. For example, the duration of snowmelt at SHEBA was over 2 weeks as opposed to 7–10 days near Barrow. The more

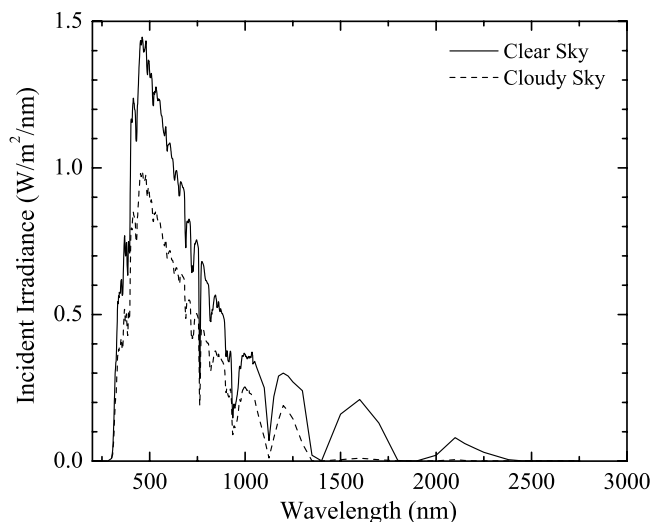


Figure 11. Incident spectral irradiance for clear and continuous stratus cloud cover. Between 300 and 1040 nm, observations have been smoothed with a 7-point running average. From 1050 to 2400 nm, the wavelength resolution was 50 nm.

rapid progress of the melt at Barrow was primarily due to the presence of adjacent land and also to the slightly lower latitude. This combination also gave rise to quicker and more intense temporal variations. As a result, while the distinct evolutionary stages described by *Perovich et al.* [2002] to characterize the albedo evolution during SHEBA were present in the coastal zone, the transitions occurred rapidly and the stages were masked to a large extent by the effects of synoptic weather fluctuations.

[48] The candling of melting fresh ice on Imikpuk Lake modifies the hydrological distribution of meltwater on the ice. The water no longer collects on the surface, can readily sink to the base of the candled layer, and can also move laterally quite efficiently. This results in a significant reduction in the area covered by melt ponds and a correspondingly higher average albedo. During the 2002 experiment, this effect was observed over large areas of sea ice where, after an early melt onset, a cold period froze solid the surface melt and flood water. When melting resumed, not only was the melt pond area decreased, but the location of individual ponds often changed. In our previous experience, particularly at SHEBA, the melt ponds varied in depth and area depending on the local hydrological balance but remained in the same place. In a more unstable regime, which might be expected during climatic warming, an early melt onset followed by substantial cooling events may be commonplace. This scenario could result in restructuring and/or reduction of the melt pond coverage particularly over undeformed ice and should be considered in modeling such situations.

4.1. Satellite Albedos

[49] Satellite imagery from MODIS has been produced for the polar regions for several years with surface resolutions from 250 m to 1 km in 36 wavelength bands, 20 of which fall in the visible and solar infrared. To provide a ground-based reference for imagery in the region studied

here, we present in Table 4 a compilation of the MODIS albedos derived from the site specific spectral albedos shown in Figure 10 for each of the MODIS channels covered by our instrument. Each value was generated using equation (2) but integrated over the bandwidth of the particular channel. The values shown were calculated using the clear-sky incident irradiance spectrum corresponding to conditions when the surface would be visible.

4.2. Cumulative Absorbed Shortwave Radiation

[50] The cumulative absorbed shortwave radiation is a major contribution to the surface heat balance. Once the snow has melted away, differential heat absorption can produce both short- and intermediate-range effects. The melt back of ice in close proximity to land is accelerated by the enhanced warming of the soil and of the resulting meltwater that builds up in long cracks or moats oriented parallel to the shoreline. Lateral advection of heat from the tundra can also affect the mass balance of the nearshore ice, enhancing melting with a corresponding cooling of the land.

[51] To evaluate the potential for such an exchange, we have calculated the total shortwave radiative energy, F_{abs} , absorbed by the surface at each observation site using equation (3). For the incident shortwave radiation, we have used daily totals for 2000, 2001, and 2002 kindly provided by R. S. Stone and E. G. Dutton (personal communication, 2003) through the auspices of NOAA/CMDL. Albedo values at the ice sites after the disappearance of the ice were taken to be 0.07, the value for open water. The integral was carried out from 1 January through 11 August for each year, covering the period for which the surface albedos are available.

$$\int_0^t [1 - \alpha(t')] \cdot F_0(t') dt' \quad (3)$$

[52] The results are presented in Figure 13. Total absorbed shortwave radiation through 11 August in 2001 reached about 1300 MJ/m², about 170 MJ/m² larger than in 2000. This difference would provide sufficient energy to melt almost 0.60 m of ice if completely absorbed. The principal reason for the difference was the greater incident radiation in 2001, particularly during June and July (after day 150) resulting from a combination of decreased regional cloud cover and lower cloud optical thickness. Interannual variations of this magnitude are probably representative of

Table 3. Total Albedos for Clear and Cloudy Sky Conditions of the Ice Types Whose Spectral Albedos are Given in Figure 10^a

Surface Type	α [Clear]	α [Cloudy]	$\Delta\alpha$
Cold snow	0.851	0.928	0.077
Melting snow	0.607	0.678	0.071
Deteriorated melting ice	0.436	0.492	0.056
Undeteriorated melting ice	0.294	0.332	0.037
Blue-green ice	0.273	0.309	0.036
Dirty ice	0.347	0.367	0.020
Early melt pond	0.239	0.266	0.027
Late melt pond	0.129	0.141	0.012
Dry tundra	0.173	0.151	-0.022
Wet tundra	0.124	0.114	-0.010

^a $\Delta\alpha$ is the difference [α (Cloudy) - α (Clear)].

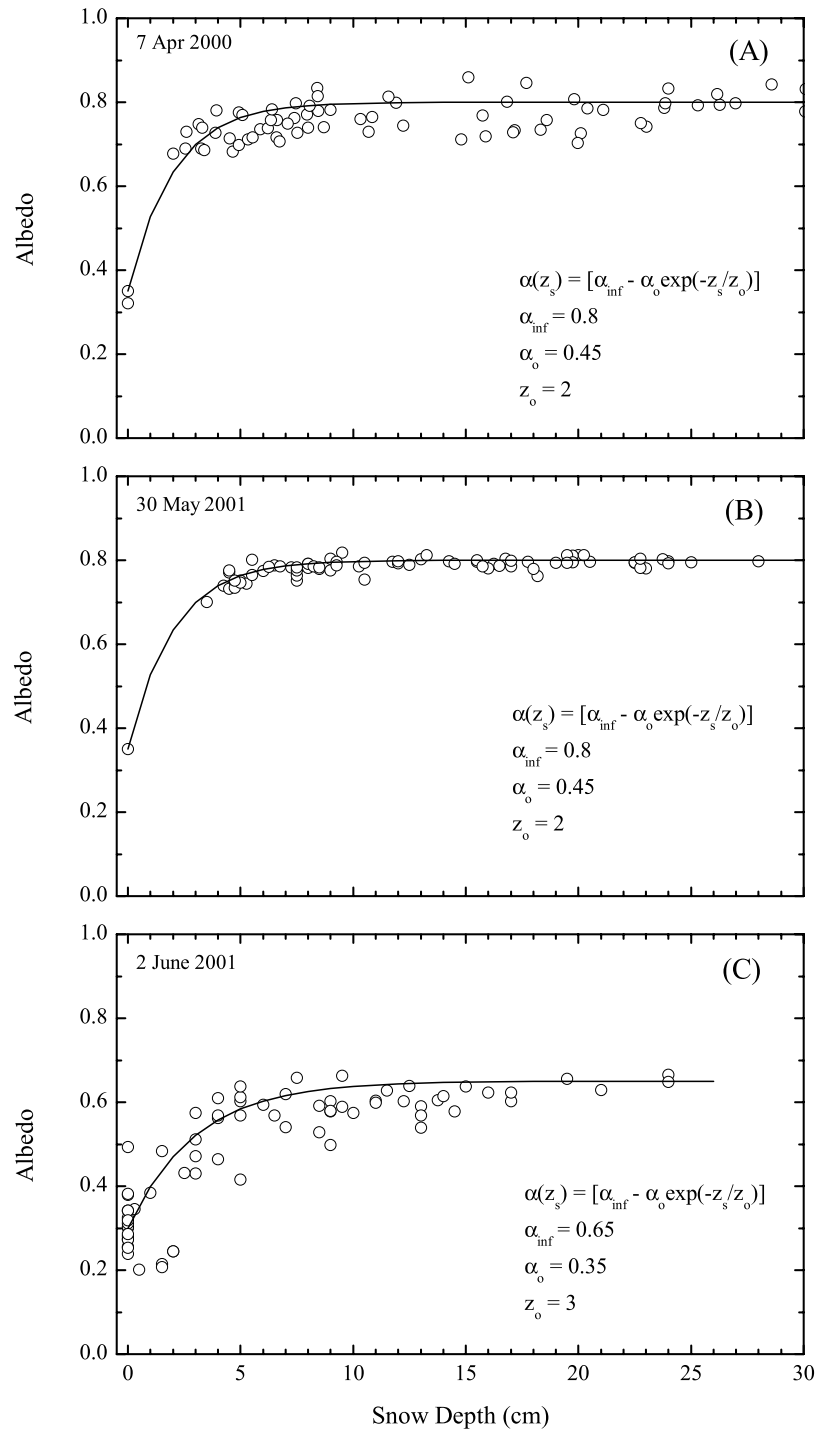


Figure 12. Total albedo versus snow depth for Imikpuk Lake prior to onset of melt in (a) 2000 and (b) 2001 and (c) just at the onset of melt in 2001. The albedo of the underlying surface is taken to be 0.35, 0.35, and 0.30 for Figures 12a, 12b, and 12c, respectively. The solid line is an exponential fit using the formula in the legend.

the area. The results for leads, whose albedo were taken to be 0.07, were about twice as large as for the ice and tundra surfaces.

[53] Excluding the tundra site in 2002, intersite differences on 11 August 2000 spanned 70 to 120 MJ/m². This corresponds to a differential equivalent ice melt of about 0.25–0.40 m. Although the span was quite similar from

year to year, the results at the individual sites were not always in the same order. This reflects differences in local processes such as the entrainment of sediment into the ice on Elson Lagoon in 2000. We feel that this span is representative of the usual interannual variability.

[54] In 2002 there was an extreme excursion when the snowmelt took place in mid-May resulting in removal of

Table 4. Albedos Integrated Over the Visible and Solar Infrared MODIS Satellite Bands^a

Band Wavelength [Average], nm	Cold Snow	Melting Snow	Deter. Melting Ice	Undeter. Melting Ice	Blue-Green Ice	Early Melt Pond	Late Melt Pond	Dirty Ice	Dry Tundra	Wet Tundra
620–670 [645]	0.981	0.756	0.572	0.378	0.335	0.255	0.162	0.412	0.117	0.079
841–876 [858.5]	0.949	0.642	0.369	0.220	0.197	0.101	0.073	0.402	0.269	0.233
459–479 [469]	0.971	0.765	0.625	0.440	0.431	0.418	0.188	0.355	0.055	0.033
545–565 [555]	0.983	0.767	0.641	0.451	0.456	0.405	0.215	0.400	0.085	0.053
1230–1250 [1240]	0.538	0.169	0.035	0.033	0.018	0.056	0.049	0.243	0.410	0.299
1628–1652 [1640]	0.168	0.023	0.008	0.014	0.005	0.044	0.038	0.161	0.355	0.182
2105–2155 [2130]	0.111	0.014	0.006	0.011	0.003	0.035	0.034	0.154	0.213	0.091
405–420 [412.5]	0.952	0.760	0.587	0.404	0.367	0.381	0.162	0.317	0.036	0.023
438–448 [443]	0.964	0.764	0.612	0.428	0.408	0.406	0.178	0.341	0.047	0.029
483–493 [488]	0.975	0.766	0.633	0.446	0.443	0.423	0.193	0.364	0.060	0.036
526–536 [531]	0.981	0.767	0.645	0.456	0.464	0.420	0.210	0.389	0.076	0.047
546–556 [551]	0.983	0.767	0.642	0.452	0.459	0.408	0.214	0.398	0.083	0.052
662–672 [667]	0.981	0.750	0.555	0.359	0.311	0.226	0.147	0.413	0.123	0.085
673–683 [678]	0.982	0.749	0.549	0.353	0.304	0.216	0.142	0.413	0.127	0.088
743–753 [748]	0.976	0.712	0.479	0.293	0.245	0.135	0.085	0.410	0.198	0.152
862–877 [869.5]	0.939	0.625	0.345	0.199	0.186	0.096	0.072	0.399	0.275	0.241
890–920 [905]	0.907	0.576	0.287	0.173	0.158	0.084	0.068	0.382	0.295	0.264
931–941 [936]	0.895	0.552	0.268	0.162	0.148	0.083	0.064	0.366	0.308	0.275
915–965 [940]	0.895	0.543	0.259	0.159	0.144	0.082	0.065	0.368	0.310	0.275
1360–1390 [1375]	0.514			0.012						

^aColumn one gives the channel designation and the spectral band limits. The center of each band is in brackets.

most of the snow cover by the beginning of June. This was the earliest melt onset on record [Stone *et al.*, 2002; K. Toovak, personal communication, 2002]. The melt was followed by a cooling period during which time the melt-water on the ice refroze and the ice albedo increased, compensating somewhat for the early melt onset; however, the tundra remained bare with a low albedo. In this case, the shortwave radiation absorbed by the ice on 11 August reached 1400 to 1500 MJ/m², and the tundra absorbed nearly 1850 MJ/m², a 42% increase over 2001. Determination of the actual partitioning of the shortwave energy and its implications for lateral and bottom melting are beyond the scope of the present work and require detailed analysis [see, e.g., Maykut and Perovich, 1987; Perovich and Maykut, 1990; Steele, 1992]. While the 2002 event is unusual, it demonstrates the extreme sensitivity of the coastal ice environment to small changes in the length of the melt season and provides insights needed for the

extension of the modeling of ice melt/decay processes in response to climate warming.

5. Conclusions

[55] As the melt season progressed, there was a general decrease in the albedo due to the melting of the snow cover and the decay of the ice. As in the central pack, synoptic weather events including refreezing, snowfall, warming, and rainfall produced abrupt perturbations and transitions in the seasonal evolution of albedo, particularly near the beginning of melt.

[56] The overall decrease of albedo proceeded considerably more rapidly than in the central Beaufort Sea as reported for the SHEBA experiment in 1998. This suggests the action of positive feedback processes causing sea ice in the coastal environment to melt faster. The disappearance of the ice was, of course, not purely a local thermodynamic phenomenon but

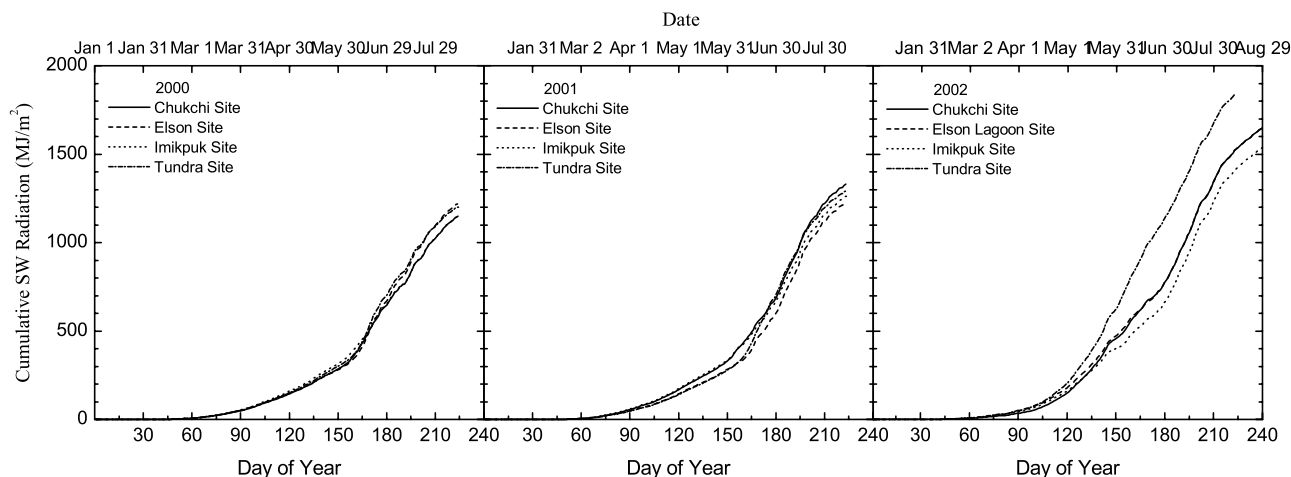


Figure 13. Cumulative absorbed shortwave radiation at the four observation sites from 1 January through 11 August 2000 and 2001. Also included are the results for an open water surface with an albedo of 0.07.

included interactive influences of heat advection, ice motion and lateral ablation of the ice floes over a wide area.

[57] During the melt, the spectral albedos for snow and ice surfaces decreased at all wavelengths and the spatial variability of the albedo increased sharply as the snow cover became patchy. The spectral albedo of tundra contrasted sharply with that of snow and ice. It increased from values less than 0.05 at 400 nm to a pair of maxima at 1100 and 1300 nm with a secondary maximum at 1670 nm. Beyond 1400 nm, tundra albedos exceeded the values for all the snow and ice cases except for dirty ice, where the dirt component was dominant. As a result, the sign of the spectral gradient ($d\alpha/d\lambda$) between about 600 and 1000 nm is opposite for ice and snow versus tundra and dirt. The surface types included in this study spanned the range encountered in the Arctic coastal zone and should provide a solid basis for interpreting MODIS and other visible and near-infrared satellite imagery of the region.

[58] The thickness of the surface scattering layer on bare ice tends to maintain itself by balancing the surface ablation with internal volume melting such that the albedo remains nearly constant, as was found during SHEBA by Perovich *et al.* [2002]. This is a stabilizing process or negative feedback with regard to the melting of drained ice. As a result, the temporal evolution of the albedo of melting sea ice is driven by the albedos and area coverage of melt ponds and by the amount of open water.

[59] The record early melt in May 2002 was followed by a pronounced freezing event 2 weeks later in which the melt ponds and flood water froze completely. This produced a distinct melt regime that gave rise to reduced melt pond coverage and higher albedo that could have a significant impact on the progress of the melt season, providing a negative feedback mechanism similar to the maintenance of the surface scattering layer on drained bare ice. Such events provide insight into secondary processes associated with the melt ponds that are necessary for modeling the energy balance of sea ice in a warming climate.

[60] The cumulative absorbed shortwave radiation is modulated by the temporal variations of albedo and local cloud cover. It provides a substantial fraction of the energy expended in melting the ice, but additional processes, both dynamic and thermodynamic, are needed to explain the local mass balance.

[61] **Acknowledgments.** This work was funded by the National Science Foundation Arctic System Science program on Grant OPP 9910300. Additional support was provided by the Department of the Army. We appreciate the excellent field support supplied by D. Ramey, the Barrow Arctic Science Consortium, and VECO. We would like to thank J. Richter-Menge, M. Sturm, B. Elder, K. Ligett, K. Claffey, C. Taylor, and S. Holmstock for their contributions to the field efforts. We are grateful to H. Eicken, B. Light, and C. George for several helpful discussions and critiques of this effort. We are indebted to R. S. Stone, T. Mefford, E. G. Dutton, and D. Longenecker and NOAA/CMDL for making available their time series of incident shortwave radiation fluxes and meteorological observations.

References

- Allison, I., R. E. Brandt, and S. G. Warren (1993), East Antarctic sea ice: Albedo, thickness distribution, and snow cover, *J. Geophys. Res.*, **98**, 12,417–12,429.
- Bond, T. C., T. L. Anderson, and D. Campbell (1999), Calibration and intercomparison of filter-based measurements of visible light absorption by aerosols, *Aerosol Sci. Technol.*, **30**, 582–600.
- Buckley, R. G., and H. J. Trodahl (1987), Scattering and absorption of visible light by sea ice, *Nature*, **326**, 867–869.

- Clarke, A. T., and K. J. Noone (1985), Soot in the arctic snowpack: A cause for perturbations in radiative transfer, *Atmos. Environ.*, **19**, 2045–2053.
- Curry, J. A., J. L. Schramm, and E. E. Ebert (1995), On the sea ice albedo climate feedback mechanism, *J. Clim.*, **8**, 240–247.
- Grenfell, T. C. (1983), A theoretical model of the optical properties of sea ice in the visible and near infrared, *J. Geophys. Res.*, **88**, 9723–9735.
- Grenfell, T. C. (1991), A radiative transfer model for sea ice with vertical structure variations, *J. Geophys. Res.*, **96**, 16,991–17,001.
- Grenfell, T. C., and G. A. Maykut (1977), The optical properties of ice and snow in the Arctic Basin, *J. Glaciol.*, **18**, 445–463.
- Grenfell, T. C., and D. K. Perovich (1984), Spectral albedos of sea ice and incident solar irradiance in the southern Beaufort Sea, *J. Geophys. Res.*, **89**, 3573–3580.
- Grenfell, T. C., S. G. Warren, and P. C. Mullen (1994), Reflection of solar radiation by the Antarctic snow surface at ultraviolet, visible, and near-infrared wavelengths, *J. Geophys. Res.*, **99**, 18,669–18,684.
- Grenfell, T. C., B. Light, and M. Sturm (2002), Spatial distribution and radiative effects of soot in the snow and sea ice during the SHEBA experiment, *J. Geophys. Res.*, **107**(C10), 10.1029/2000JC000414.
- Hanesiak, J. M., D. G. Barber, R. A. De-Abreu, and J. J. Yackel (2001), Local and regional albedo observations of Arctic first-year sea ice during melt ponding, *J. Geophys. Res.*, **106**, 1005–1016.
- Langleben, M. P. (1969), Albedo and degree of puddling of a melting cover of sea ice, *J. Glaciol.*, **8**, 407–412.
- Langleben, M. P. (1971), Albedo of melting sea ice in the southern Beaufort Sea, *J. Glaciol.*, **10**, 101–104.
- Light, B., H. Eicken, G. A. Maykut, and T. C. Grenfell (1998), The effect of included particulates on the spectral albedo of sea ice, *J. Geophys. Res.*, **103**, 27,739–27,752.
- Light, B., G. A. Maykut, and T. C. Grenfell (2003), A two-dimensional Monte Carlo model of radiative transfer in sea ice, *J. Geophys. Res.*, **108**(C7), 3219, doi:10.1029/2002JC001513.
- Maykut, G. A., and D. K. Perovich (1987), The role of shortwave radiation in the summer decay of a sea ice cover, *J. Geophys. Res.*, **92**, 7032–7044.
- Maykut, G. A., and N. Untersteiner (1971), Some results from a time-dependent thermodynamic model of sea ice, *J. Geophys. Res.*, **76**, 1550–1576.
- Morison, J., et al. (2001), Search: Study of environmental Arctic change, 85 pp., Univ. of Washington, Seattle.
- Parkinson, C. L., D. J. Cavalieri, P. Gloersen, H. J. Zwally, and J. C. Comiso (1999), Arctic sea ice extents, areas, and trends, 1978–1996, *J. Geophys. Res.*, **104**, 20,837–20,856.
- Pegau, W. S., and C. A. Paulson (2001), The albedo of Arctic leads in summer, *Ann. Glaciol.*, **33**, 221–224.
- Perovich, D. K. (1991), Seasonal changes in sea ice optical properties during fall freezeup, *Cold. Reg. Sci. Technol.*, **19**, 261–273.
- Perovich, D. K. (1994), Light reflection from sea ice during the onset of melt, *J. Geophys. Res.*, **99**, 3351–3359.
- Perovich, D. K. (1996), *The Optical Properties of Sea Ice*, CRREL Monogr., vol. 96-1, 25 pp., Cold Reg. Res. and Eng. Lab., Hanover, N. H.
- Perovich, D. K., and T. C. Grenfell (1981), A theoretical model of radiative transfer in young sea ice, *J. Glaciol.*, **27**, 331–346.
- Perovich, D. K., and G. A. Maykut (1990), Solar heating of a stratified ocean in the presence of a static ice cover, *J. Geophys. Res.*, **95**, 18,233–18,245.
- Perovich, D. K., T. C. Grenfell, B. Light, and P. V. Hobbs (2002), Seasonal evolution of Arctic sea-ice albedo, *J. Geophys. Res.*, **107**(C10), 8044, 10.1029/2000JC000438.
- Radionov, V. F., N. N. Bryazgin, and E. I. Alexandrov (1997), The snow cover of the Arctic Basin, *APL-UW Tech. Rep. 9701*, Appl. Phys. Lab., Univ. of Wash., Seattle.
- Rothrock, D. A., Y. Yu, and G. A. Maykut (1999), Thinning of the Arctic sea ice cover, *Geophys. Res. Lett.*, **26**, 3469–3472.
- Steele, M. (1992), Sea ice melting and floe geometry in a simple ice-ocean model, *J. Geophys. Res.*, **97**, 17,729–17,738.
- Stone, R. S., E. G. Dutton, J. M. Harris, and D. Longenecker (2002), Earlier spring snowmelt in northern Alaska as an indicator of climate change, *J. Geophys. Res.*, **107**(10), 4089, doi:10.1029/2000JD000286.
- Warren, S. G., and W. J. Wiscombe (1980), A model for the spectral albedo of snow. II: Snow containing atmospheric aerosols, *J. Atmos. Sci.*, **37**, 2734–2745.
- Warren, S. G., and W. J. Wiscombe (1985), Dirty snow after nuclear war, *Nature*, **313**, 467–470.
- Wiscombe, W. J., and S. G. Warren (1980), A model for the spectral albedo of snow. I: Pure snow, *J. Atmos. Sci.*, **37**, 2712–2733.

T. C. Grenfell, Department of Atmospheric Sciences, Box 351640, University of Washington, Seattle, WA 98195, USA. (tcg@atmos.washington.edu)

D. K. Perovich, ERDC-CRREL, 72 Lyme Road, Hanover, NH 03755, USA.

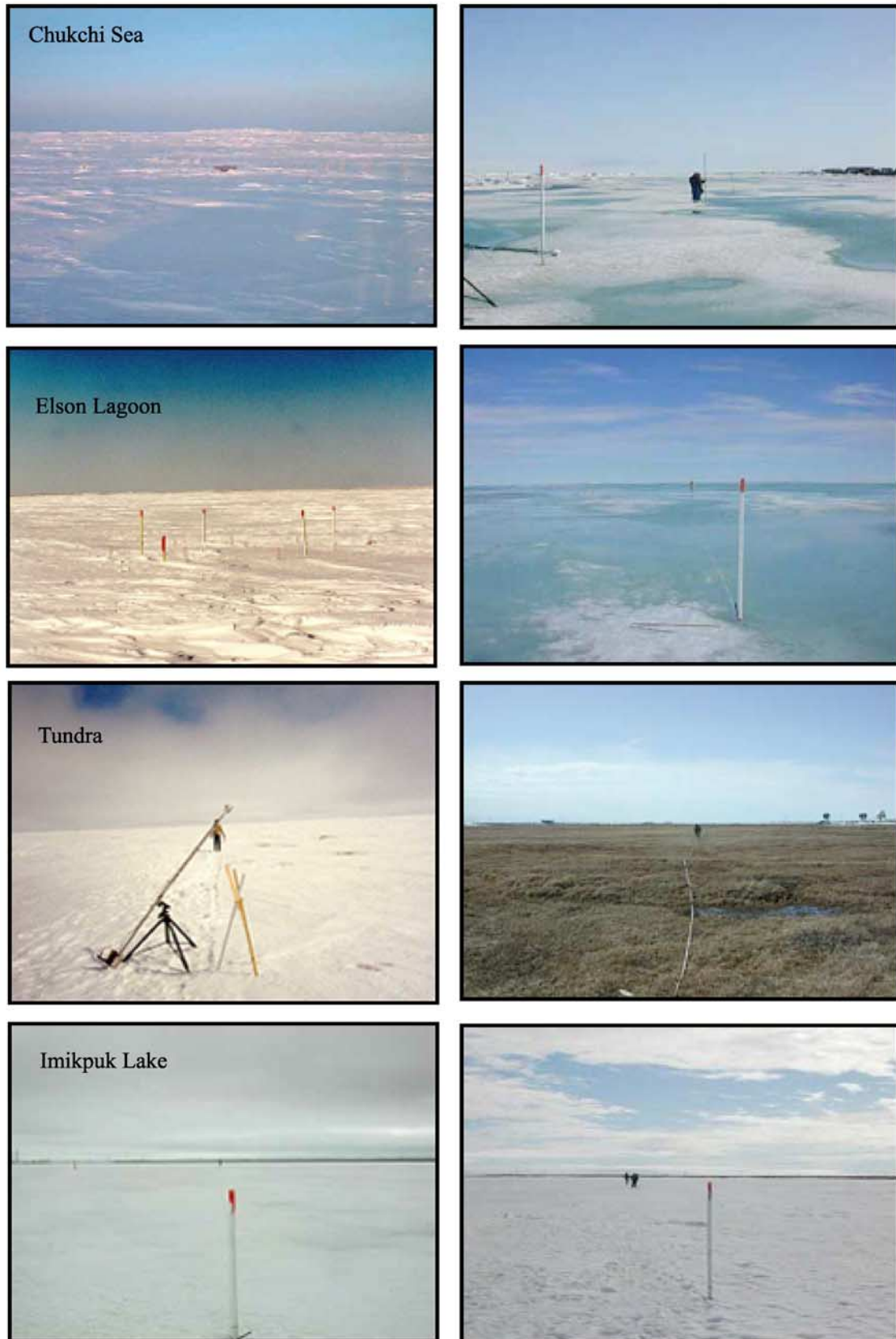


Figure 2. Photographs of the four albedo sites illustrating conditions during the growth and melt seasons.

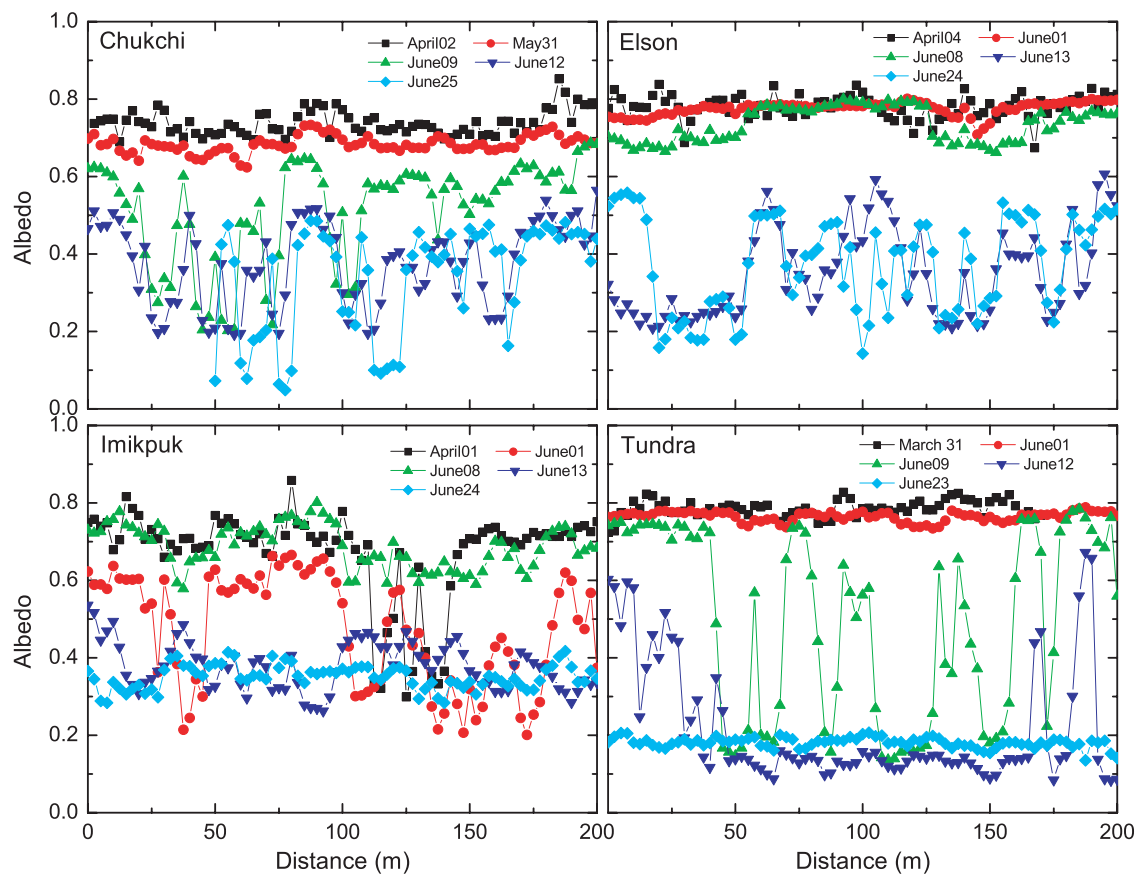


Figure 5. Spatial variability of albedo observed at the four sites during the spring-summer 2001. Imikpuk Lake has the lowest April albedo since it has the thinnest snow cover.

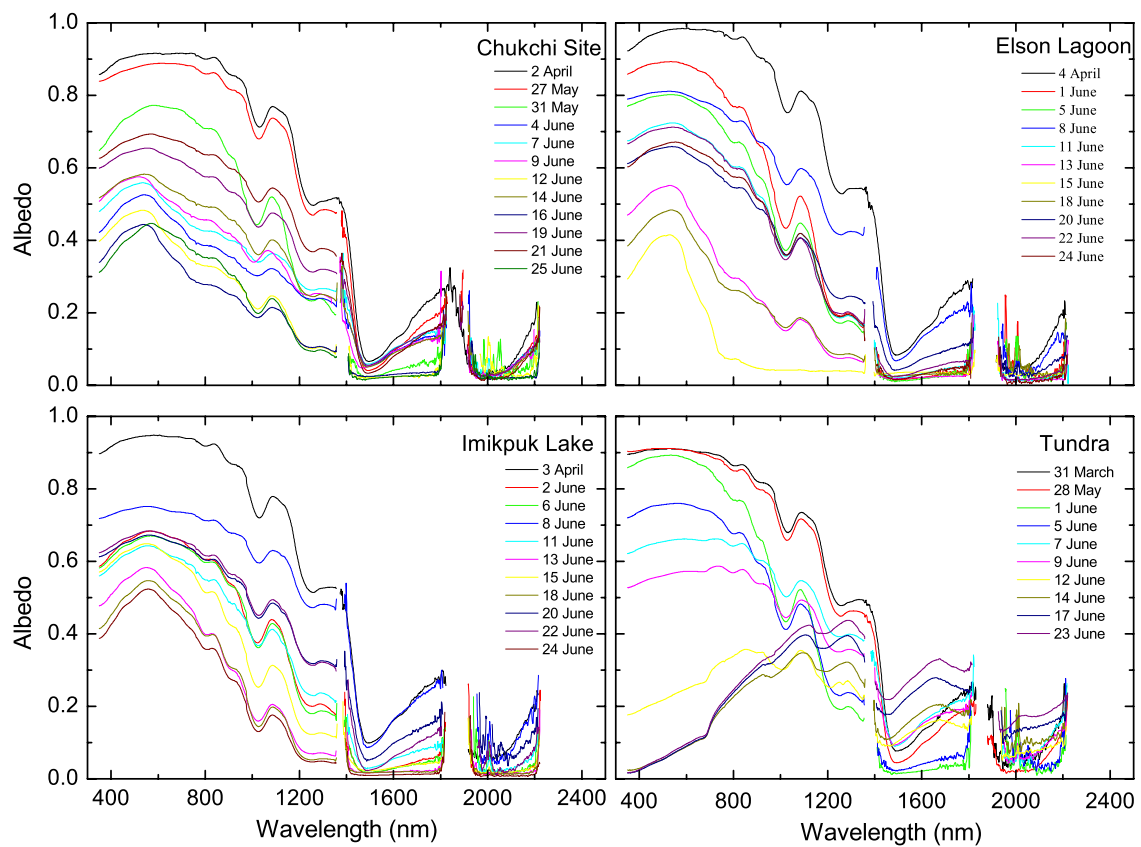


Figure 8. Evolution of mean spectral albedo at the four sites. Each curve represents the averaged value of albedo over a 200-m-long line. The decrease as the melt season develops is clearly apparent.